Green Chemistry

PAPER

View Article Online
View Journal

Cite this: DOI: 10.1039/d5gc06439b

Ru/TiO_2 catalysts for selective formation of ring hydrogenation or ring-opening products from biomass-derived 5-hydroxymethylfurfural

Preeti Kashyap,[a] Marcin Jędrzejczyk,[a] Mingjun Gu,[b] Stephan N. Steinmann,[c] David Kubička,[d] Nicolas Keller,[e] Carine Michel *[c] and Agnieszka M. Ruppert *[a]

Received 30th November 2025,
Accepted 3rd February 2026

DOI: 10.1039/d5gc06439b

rsc.li/greenchem

We report for the first time a one-pot catalytic route for the selective hydrogenation of biomass-derived 5-hydroxymethylfurfural (HMF) into 1,2,5-hexanetriol and related value-added products such as 1-hydroxyhexane-2,5-dione (HHD) and 2,5-bis(hydroxymethyl)tetrahydrofuran (BHMTHF) using a Ru/TiO_2 catalyst. In particular, the influence of the solvent composition (water–dioxane) on the reaction pathways for HMF ring opening and ring reduction products was investigated, revealing that water acts not only as a sustainable solvent but also as a reactive substrate, promoting OH-group rearrangements. Under optimized conditions, BHMTHF was obtained in >99% yield in pure 1,4-dioxane, while HHD and 1,2,5-hexanetriol were produced at 90% and 75% yields, respectively, in pure aqueous media. DFT calculations on Ru (0001) surfaces indicate that water increases the concentration of surface hydroxyl species (OH*), facilitating selective ring-opening reactions. Catalyst characterization showed minor increases in Ru particle size and solvent-dependent metallic Ru availability, influenced by carbon deposition. Nevertheless, the Ru/TiO_2 catalyst retained high activity and selectivity over several cycles in both solvents. This study demonstrates a solvent-directed, highly selective strategy for converting HMF into valuable chemicals, integrating experimental and theoretical insights to advance green catalytic processes.

Green foundation

1. Our work advances green chemistry by establishing the first solvent-directed, one-pot catalytic route enabling tunable and highly selective conversion of biomass-derived HMF into three valuable products that are 1,2,5-hexanetriol, 1-hydroxyhexane-2,5dione and 2,5-bis(hydroxymethyl)tetrahydrofuran using a recyclable Ru/TiO_2 catalyst.

2. The key green achievement is the demonstration that water – an abundant, renewable, and benign solvent – acts not only as the reaction medium but also as reactive participant, enabling –OH group rearrangements and affording high yields, including an unprecedented 75% yield of 1,2,5-hexanetriol in pure water. Supported by mechanistic insight from DFT calculations that rationalize solvent-controlled selectivity, this onepot strategy eliminates multistep processing and significantly minimizes waste.

3. Greener performance could be further achieved by replacing Ru with earth-abundant metals, further improving the catalyst resistance to carbon deposition, and coupling the reaction with renewable hydrogen sources through transfer hydrogenation from green donors.

1. Introduction

Derived from biomass, 5-hydroxymethylfurfural (HMF) is a key platform compound whose versatile multifunctional structure enables its straightforward transformation into a variety of high-value derivatives, thereby offering broad opportunities for sustainable chemical production. Through selective catalytic transformations, HMF can be converted into a wide range of value-added chemicals, including 2,5-dimethylfuran (DMF),[1] 5-methylfurfurylalcohol (5-MFA), 2,5-bishydroxymethylfuran (BHMF),[2] 2,5-bishydroxymethyltetrahydrofuran (BHMTHF),[3] hexanetriols, hexanediols, and related compounds.[4,5] Since

[a]Institute of General and Ecological Chemistry, Faculty of Chemistry, Lodz University of Technology Żeromskiego 116, 90-924 Lodz, Poland.
E-mail: agnieszka.ruppert@p.lodz.pl
[b]ENS de Lyon, CNRS, LCH, UMR 5182, 69342 Lyon cedex 07, France
[c]CNRS, ENS de Lyon, LCH, UMR 5182, 69342 Lyon cedex 07, France.
E-mail: carine.michel@ens-lyon.fr
[d]Department of Sustainable Fuels and Green Chemistry, University of Chemistry and Technology Prague, Technická 5, 166 28 Prague, Czech Republic
[e]Institut de Chimie et Procédés pour l'Energie, l'Environnement et la Sante (ICPEES), CNRS, University of Strasbourg, 25 rue Becquerel, 67087 Strasbourg, France

HMF is not volatile, its catalytic conversion is typically carried out in the liquid phase under H_2 pressure using metal-based catalysts capable of activating the H–H bond. Catalytic hydrodeoxygenation plays a pivotal role in HMF conversion, as it enables the removal of oxygen functionalities *via* hydrogenation and dehydration reactions. However, liquid phase hydrodeoxygenation of HMF is intrinsically challenging due to the coexistence of multiple reactive sites (C═O, C–OH, and the furan ring), which often lead to competing pathways and poor selectivity among ring-hydrogenated, partially-deoxygenated, and ring-opened products.

Scheme 1 illustrates the hydrodeoxygenation pathway of HMF, in which the selective hydrogenation of the aldehyde group initially produces BHMF. From BHMF, three main reaction routes are possible: (i) direct hydrogenation of the furan ring to form BHMTHF; (ii) hydrodeoxygenation through selective removal of one hydroxyl group to form 5-MFA; or (iii) direct ring opening to generate 1-hydroxyhexane-2,5-dione (HHD). HHD can subsequently undergo hydrogenation to produce 1,2,5-hexanetriol (1,2,5-HT), or intramolecular aldol condensation to form 3-(hydroxymethyl)cyclopentanol (HCPO). Further dehydration of 1,2,5-HT leads to the formation of hexanediols, as depicted in Scheme 1. All these compounds have wide applications in the polymer and pharmaceutical industries. In particular, HHD serves as a key precursor for 3-methyl-2-cyclopentenone, a commercially valuable compound widely used in the flavor and fragrance industries. Meanwhile, 1,2,5-HT is a versatile building block in organic synthesis. It can undergo esterification, etherification, and various other transformations to yield a wide range of functionalized derivatives such as plasticizers, surfactants, and resins. Additionally, 1,2,5-HT can also serve as a monomer in polymerization reactions to synthesize polyesters and polyethers.[6–8]

For example, Luijk *et al.* and Yang *et al.* achieved selective HHD synthesis using Pd/C catalysts in water with added hydrochloric or acetic acid, respectively, highlighting the essential role of external acids and solvent polarity in promoting ring-opening reactions.[9,10] Similarly, Liu and co-workers reported that Pd/C in CO_2/H_2O (forming *in situ* carbonic acid) efficiently promoted ring-opening to HHD, whereas in the absence of CO_2, only BHMF and BHMTHF were obtained, indicating the necessity of in-built carbonic acid to facilitate ring opening.[11] These findings demonstrate that acidic environments in the presence of water are crucial for furan ring-opening, though reliance on external acids limits practical efficiency. On the other hand, single-atom Pd catalysts as well as their gold-promoted analogues supported on acidic oxides such as Nb_2O_5 underscore the remarkable potential of atomically dispersed metals. The interplay between single-atom active sites, surface acidity, and the protic medium drives highly selective HMF ring-opening.[12,13]

Recently, Ru supported on activated biochar was shown to exhibit high activity in water, achieving 100% HMF conversion and 88% HHD yield.[14] This performance was initially attributed to a synergistic balance between Brønsted acidity – arising from carboxyl, phenolic, and lactone groups and Lewis acidity provided by the Ru sites. The influence of acidity was further confirmed by adding an external acid source, namely formic acid, which enhanced both activity and selectivity toward HHD, underscoring the importance of controlled external acidity sources. Subsequently, Polidoro *et al.*[15] developed a multiphase system (water/isooctane/ionic liquid) using commercial Ru/C, where catalyst migration to the organic phase slowed down HMF ring saturation, consequently favoring BHMF formation. The introduction of an acidic ionic liquid layer subsequently promoted HHD synthesis *via* BHMF ring opening. While these studies clearly emphasized the influence of acid and water, the precise mechanistic role of water remains unclear. Additionally, despite Ru catalysts are known for their superior hydrogenation ability and high activity in protic environments, attributed to their lower activation barrier for carbonyl hydrogenation,[16,17] their potential for promoting the ring-opening conversion of HMF remains largely unexplored.

Moreover, while valuable research has been conducted on HHD formation, its further hydrogenated product, 1,2,5-HT, has received little attention, leaving its potential largely

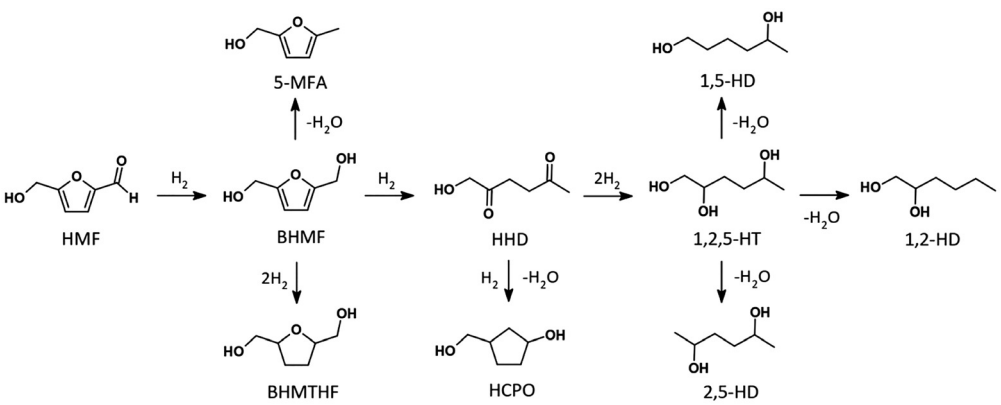

Scheme 1 HMF hydrogenation reaction pathway.

untapped. This gap arises from the intrinsic complexity of directly hydrogenating HHD under aqueous acidic conditions. Both carbonyl and hydroxyl groups are prone to various competing side reactions, including aldol condensation, dehydration, etherification, acetal formation, and even polymerization. Consequently, achieving high selectivity toward the direct hydrogenative conversion of HHD to 1,2,5-HT in a one-pot process is highly challenging. To the best of our knowledge, no report has demonstrated a one-pot synthesis of 1,2,5-HT directly from HMF. The only notable attempt was described by Zhang *et al.*, who used a two-step approach in which HMF was first converted to HHD over a Pt/C catalyst, followed by a separate hydrogenation step using Ru/C in water to obtain 1,2,5-HT.[8]

In this study, we report the selective one-pot synthesis of 1,2,5-HT directly from HMF using a Ru/TiO_2 catalyst. Titania was selected as a reducible support owing to its chemical and thermal stability under hydrothermal and acidic conditions, its tunable metal–support interactions[18] that enable fine-tuning of catalytic performance, and its ability to promote high metal dispersion leading to the formation of ultrasmall crystallites.[2] While the influence of water on hydrodeoxygenation pathways has been noted previously, we conducted a comprehensive investigation to elucidate its mechanistic role in governing product selectivity. Systematic experiments revealed that the solvent composition critically determines the reaction pathway, with water promoting routes leading to ring-opened products such as HHD, whereas pure organic solvents like dioxane favor initial ring hydrogenation, yielding predominantly BHMTHF. Extensive post-reaction catalyst characterization, together with complementary DFT calculations, provided molecular-level insight into how water facilitates the formation of ring-opened intermediates and products that are otherwise inaccessible in purely organic media.

2. Experimental section

2.1 Materials and chemicals

5-Hydroxymethylfurfural (98%) was obtained from Fluorochem Ltd (UK), and 1,4-dioxane (99.8%) was purchased from Sigma Aldrich (Germany). $RuCl_3{\cdot}3H_2O$, used as the metal precursor, was supplied by Sigma Aldrich. The anatase-rutile mixed-phase Aeroxide© TiO_2 P25 was provided by Evonik-Degussa (Germany).

2.2 Ru/TiO_2 synthesis

Ru/TiO_2 catalyst with 1 wt% Ru loading was prepared *via* the wet impregnation method. In a typical synthesis, 2.97 g of TiO_2 support was dispersed under stirring in 40 mL of an aqueous Ru precursor solution at the desired concentration. The resulting catalyst suspension was aged at room temperature for 24 h. After solvent evaporation, the catalyst was dried at 120 °C for 2 h. Finally, the dried sample was reduced under a H_2 flow at 400 °C for 1 h, using a heating ramp of 20 °C min^{-1}. Those are the standard reaction conditions if not stated differenty. Inductively coupled plasma (ICP) analysis confirmed a Ru content of 0.99 wt%, in good agreement with the targeted value.

2.3 Density functional theory (DFT) calculations

DFT calculations were carried out using the Vienna Ab Initio Simulation Package (VASP) to determine reaction energies and activation barriers. The electronic structures and interactions were described using the Perdew, Burke, and Ernzerhof (PBE) exchange–correlation functional within the generalized gradient approximation (GGA) framework, complemented with a dispersion correction (dDsC). A plane-wave energy cutoff of 400 eV was used, and the convergence criteria for the electronic energy were set to 10^{-6} eV. The Brillouin zone sampling was performed using a 3 × 3 × 1 Monkhorst–Pack *K*-point grid for surface calculations, while bulk calculations were done utilizing a denser 19 × 19 × 19 grid. The hexagonal close-packed (hcp) Ru lattice constant (a) was determined to be 2.68 Å with a c/a ratio of 1.633. The Ru(0001) metal surface was modelled using a $p(4 \times 4)$ slab comprising four atomic layers, with a 20 Å vacuum layer to prevent interactions between periodic slabs. The bottom two layers were fixed at their bulk interatomic distances, while the coordinates of the top two layers and of all adsorbates were fully relaxed till the maximal force was below 0.02 eV $Å^{-1}$. Frequencies are evaluated within the harmonic approximation for the degrees of freedom that were free to relax.

Transition states (TS) were optimized at the same level of numerical accuracy using a combination of nudge elastic band and dimer methods and confirmed by the presence of only one imaginary frequency corresponding to the reaction coordinate of the elementary step. Adsorption energies (E_{ads}) for reactants and products on the Ru(0001) surface were calculated using the following equation:

$$E_{ads} = E_{total} - E_{surface} - E_{absorbate}$$

where E_{total}, $E_{surface}$, and $E_{absorbate}$ represent the total energy of the system, clean surface, and isolated adsorbate, respectively. The activation energy (E_a) of the reaction was calculated using the equation:

$$E_a = E_{TS} - E_{IS}$$

where E_{TS} denotes the energy of the TS, and E_{IS} corresponds to the energy of the initial state (IS).

Moreover, the Gibbs free energy corrections were evaluated under experimental conditions of T = 393.15 K and p = 1 atm. For gas-phase species, translational and rotational contributions were derived within the ideal gas and rigid rotor approximations, while vibrational contributions were obtained from the calculated harmonic frequencies. The free energy G in the gas phase was computed as:

$$\begin{aligned} G_{gas} &= H - TS = U_{elec} + PV - TS \\ &= E_{elec} + Nk_BT + ZPE - T(S_{trans} + S_{rot} + S_{vib}) \end{aligned}$$

where H is enthalpy, S is entropy, U_{elec} is the electronic energy, ZPE is the zero-point energy, and S_{vib}, S_{rot}, S_{trans} are the trans-

lational, rotational, and vibrational contributions to entropy. PV can be replaced by Nk_BT under the ideal gas assumption.

For adsorbed compounds, translational and rotational degrees of freedom are strongly hindered on the surface. Therefore, the entropy correction was restricted to vibrational contributions only. The free energy of the adsorbed state was thus approximated as:

$$G_{ads} = H - TS \approx E_{elec} + ZPE - TS_{vib}$$

To avoid overestimating the contribution to entropy of the low-frequency modes corresponding to frustrated translations, all frequencies below 50 cm^{-1} were replaced with 50 cm^{-1}.

2.4 Characterization techniques

Temperature-programmed reduction (TPR). Temperature-programmed reduction (TPR) measurements were performed on an AMI1 system (Altamira Instruments, USA) equipped with a thermal conductivity detector to examine the catalyst reducibility. Before the analysis, both fresh and spent catalysts were pre-treated *in situ* at 120 °C for 30 min under a gas mixture of 5 vol% O_2 and 95 vol% Ar. Subsequently, TPR profiles were recorded from 50 °C to 700 °C at a temperature ramp of 10 °C min^{-1} using a mixture of 5 vol% H_2 and 95 vol% Ar at a space velocity of 3.1×10^{-9} g s^{-1} cm^{-3}.

Fourier transform infrared (FTIR). Fourier transform infrared (FTIR) characterization was carried out using a Nicolet 6700 FTIR spectrometer equipped with a liquid nitrogen-cooled MCT detector to record the IR spectra of the spent materials and the spectra of adsorbed CO for the fresh and spent catalysts. IR spectra of the spent catalysts after the reaction were collected in DRIFTS mode using the Selector diffuse reflectance accessory (Specac Ltd). The spectra of adsorbed CO were collected using a DRIFTS Environmental Chamber (Specac Ltd). Prior to CO adsorption, the catalysts were *in situ* treated under a 5% H_2/Ar flow for 1 h, at 400 °C for the fresh Ru/TiO_2, and at 40 °C for the spent catalysts. After cooling to room temperature under an Ar flow, the spectra of adsorbed CO were acquired following the stepwise protocol: background collection, CO adsorption under a 5% CO/Ar flow for 20 min, purging in Ar flow for 20 min to remove unadsorbed CO, and final recording of the adsorbed CO spectrum. All spectra were recorded at a resolution of 4 cm^{-1} by collecting 128 scans.

Time-of-flight secondary ion mass spectrometry (ToF-SIMS). Time-of-flight secondary ion mass spectrometry (ToF-SIMS) analysis was carried out using an ION-TOF GmbH instrument equipped with a 25 kV pulsed Bi_3^+ primary ion gun operated in static mode to acquire secondary ion mass spectra. Prior to analysis, the samples were compressed into pellets and mounted on the sample holder using double-sided adhesive tape. The surface area analyzed for each sample was 500 μm × 500 μm. To neutralize surface charge during measurement, a pulsed low-energy electron flood gun was used, and each sample was analyzed three times to ensure reproducibility.

Transmission electron microscopy (TEM). Transmission electron microscopy (TEM) was performed using a JEOL 2100 F instrument with a point resolution of 0.2 nm. Each sample was sonicated in ethanol before a drop of the suspension was deposited onto a holey carbon membrane-coated Cu grid. The Ru nanoparticle size distributions were calculated using the ImageJ software by averaging 300 particles.

X-ray photoelectron spectroscopy (XPS). X-ray photoelectron spectroscopy (XPS) characterization was performed on a ThermoVGMultilabESCA3000 spectrometer (Al Kα anode at $h\lambda$ = 1486.6 eV). The energy shift due to electrostatic charging was subtracted using the contamination sp2 carbon C 1s band at 285.0 eV. Contributions with Doniach–Sunjic shape[19] and an S-shaped Shirley type background[20] were used, while the surface atomic ratios were obtained using the appropriate experimental sensitivity factors, as determined by Scofield.[21]

2.5 Catalytic tests

The hydrodeoxygenation of 5-hydroxymethylfurfural was performed in a 60 mL Hastelloy autoclave using 1 g of HMF, 0.15 g of catalyst, and 30 mL of solvent. Prior to the reaction, the reactor was purged twice with hydrogen and then pressurized to 70 bar with H_2. The reaction was conducted at 120 °C for the desired duration. Afterwards, the autoclave was cooled down to room temperature, and the residual pressure was released. The reaction mixture was then centrifuged to separate the catalyst from the liquid phase. The products were analyzed using an Agilent 7820A gas chromatograph equipped with a flame ionization detector and a Zebron ZB-WAXplus capillary column.

The HMF conversion and the products yield were calculated using the following formulas:

$$\text{Conversion}\,(\%) = \left(1 - \frac{n_{f(HMF)}}{n_{i(HMF)}}\right) \times 100$$

$$\text{Yield}_p(\%) = \frac{n_p}{n_{i(HMF)}} \times 100$$

where $n_{i(HMF)}$ and $n_{f(HMF)}$ are the number of moles of HMF molecules before and after the test, respectively, and n_p is the number of moles of a given product within the reaction mixture.

3. Results

3.1 Catalytic activity

We investigated the influence of the solvent on the performance of the Ru/TiO_2 catalyst in the hydrodeoxygenation of HMF. The reaction conditions (duration, pressure of H_2, and temperature) were selected based on our previous study on HMF hydrogenation in dioxane[3] and preliminary experiments in water (Table S1), optimizing the HHD yield in pure water. The product distributions obtained at different water-dioxane solvent ratios for a reaction time of 150 min are summarized in Table 1. The introduction of water into the reaction medium was found to strongly impact the product distribution. In pure dioxane, the hydrogenation of the carbonyl group of HMF occurred, and BHMF was formed as the main

Table 1 Influence of solvent ratio in HMF hydrodeoxygenation using Ru/TiO_2

	Product yield [%]						
Water : dioxane ratio (v/v)	BHMF	BHMTHF	HHD	1,2,5-HT	HCPO	Others	CB (%)
0 : 1*	93	2	0	0	0	3	97
1 : 9	31	67	0	0	0	2	98
1 : 1	0	48	0	48	1	3	97
9 : 1	0	8	56	32	3	1	99
1 : 0	2	5	83	5	4	1	99
0 : 1**	0	100	0	0	0	0	100
1 : 1**	0	54	0	27	0	19	81
1 : 0**	0	4	0	75	4	17	83

Reaction conditions: 0.15 g catalyst, 1 g HMF, 30 mL solvent, 650 rpm, 70 bar H_2, 120 °C, 150 min (**1440 min). HMF conversion reached 100% in all reaction conditions, except for *(98%). CB: The carbon balance corresponded to all products that have been detected and quantified, while "others" are the remaining non-quantified products.

product with 93% yield. The addition of a small amount of water (10 vol%) significantly promoted the further hydrogenation of the furan ring, yielding BHMTHF (67% yield). However, a further increase in the water content dramatically shifted the selectivity toward ring-opening structures such as HHD and its hydrogenated counterpart 1,2,5 HT. When equal volumes of water and dioxane (1 : 1 v/v) were used, comparable amounts of BHMTHF and 1,2,5-HT were obtained (48% yield). In contrast, with 90% water, the yields of these compounds decreased, and HHD became the main product (56% yield). Under purely aqueous conditions, the reaction was found to be highly selective for HHD, reaching 83% yield. Along with HHD, traces of BHMF, BHMTHF, 1,2,5-HT, and HCPO were also detected as byproducts. These findings suggest that the solvent plays a critical role in steering the reaction pathways. Under optimized reaction conditions, 100% BHMTHF yield was achieved in pure dioxane, while the purely aqueous system enabled the production of 1,2,5-HT with a 75% yield. Additionally, tests performed for a shorter reaction time of 60 min revealed that the presence of water positively influenced the HMF conversion, while promoting the formation of HHD and other byproducts at the expense of BHMF selectivity (Table S2). Interestingly, no significant Ru leaching was detected during the tests, regardless of the solvent composition (Table S3). The highest, though still negligible, Ru leaching (0.0041%) was observed for the pure dioxane system.

Experiments at different reaction times were conducted to gain further insight into the reaction kinetics and the product evolution. The results obtained in pure water are shown in Fig. 1, whereas we reported previously that the BHMF yield gradually decreases with prolonged reaction time in pure dioxane, accompanied by the progressive conversion to BHMTHF (see also Table 1).[3] In pure water, complete HMF conversion is reached after 140 min, corresponding to a maximum HHD yield of 90% (Fig. 1). It decreases when the reaction is prolonged, accompanied by the formation of a significant amount of unknown compounds. After 240 min of reaction, only 6% of HHD was detected along with 26% of 1,2,5-HT, while nearly 60% of the reaction products consisted of unidentified compounds. These byproducts likely originated

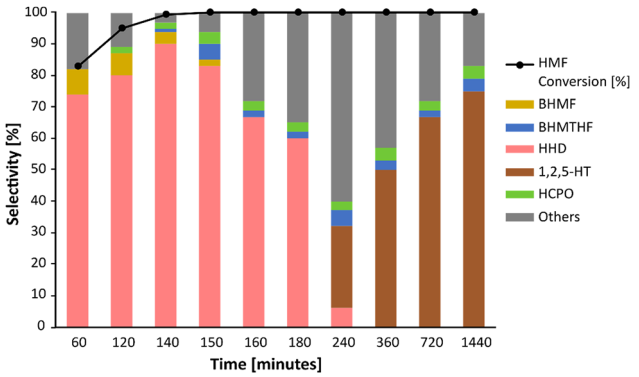

Fig. 1 Influence of reaction time on the product distribution for the HMF hydrodeoxygenation in water over Ru/TiO_2. Reaction conditions: 0.15 g catalyst, 1 g HMF, 30 mL of water, 70 bar H_2, 120 °C.

from secondary reactions, such as aldol condensation and acetal formation, which typically occur under acidic aqueous conditions. Further details on these compounds and their possible formation pathways are discussed in Section 3.3. Interestingly, extending the reaction time to 24 h in water led to a substantial increase in the 1,2,5-HT yield, reaching 75% (Table 1). In dioxane, prolonging the reaction time to 24 h resulted in 100% BHMTHF formation. By contrast, in the 1 : 1 solvent system, a longer reaction time had little impact on the BHMTHF yield, while 1,2,5-HT was formed in 27%, along with a significant amount of additional byproducts.

The recyclability of the Ru/TiO_2 catalyst was evaluated in both pure water and pure dioxane solvent over four consecutive reaction cycles, as shown in Fig. 2. The catalyst exhibited high stability, activity, and selectivity, being maintained for up to three cycles in both solvents. HMF conversion remained nearly complete, with only a slight decrease from 100% to about 94% over the first three runs, while product selectivity toward HHD in water and BHMF in dioxane remained unchanged. In the fourth cycle, the HMF conversion decreased to 85% in water and 80% in dioxane. Nevertheless, the selectivity toward the main products (HHD in water and BHMF in dioxane) remained high at around 90%. The very good performances of

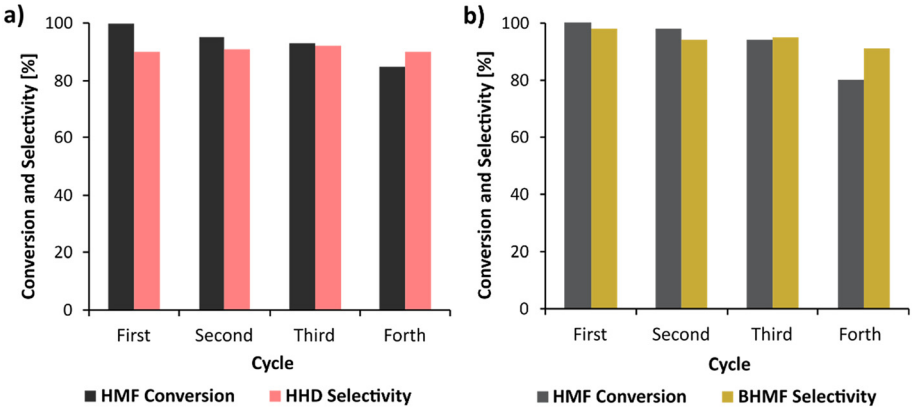

Fig. 2 Recyclability of the Ru/TiO_2 catalyst over four consecutive reaction cycles: (a) in water and (b) in dioxane. Reactions were carried out with 1 g HMF, 0.15 g catalyst, 30 mL solvent, 70 bar H_2, at 120 °C and 650 rpm; reaction times were 140 min for water and 160 min for dioxane. Detailed experimental procedures are given in Table S4.

the catalyst with cycling was accompanied by bulk structural and phase stability under high-pressure hydrogenation conditions, with no changes in anatase/rutile composition, mean crystallite size, or specific surface area, irrespective of solvent composition or number of reaction cycles (Fig. S1 and S2).

3.2 Characterization of the catalyst

Several characterization techniques were employed on both the fresh catalyst and the spent catalysts obtained after reactions in different solvents to clarify the effect of the solvent on catalyst performance.

The Ru dispersion in the fresh and spent catalysts was characterized by TEM and presented in Fig. 3 with the corresponding average Ru nanoparticle size. The fresh Ru/TiO_2 catalyst displayed a narrow size distribution with highly dispersed Ru nanoparticles and an average particle size of 1.5 nm ± 0.2 nm. The spent catalysts exhibited a slightly broader Ru nanoparticles distribution, along with a modest increase in the average Ru particle size of 1.7 nm ± 0.2 nm for the catalyst spent in pure dioxane and 1.9 nm ± 0.2 nm for the one spent in pure water. This small growth and broadening of the Ru particle size distribution can be due to the re-nucleation of Ru particles under the hydrogenation conditions.[22,23]

The FTIR spectra of CO adsorbed on fresh and spent Ru/TiO_2 catalysts were recorded to probe the accessibility of the metallic sites (Fig. 4). In the case of the fresh catalyst, three major intense bands were found. Two high-frequency bands were observed at 2133 cm^{-1} and 2070 cm^{-1}, characteristic of $Ru^{n+}(CO)_x$, where n is typically 2 to 4 and x is typically 2 or 3. A low-frequency broad-tail band peaks at 2010 cm^{-1} and is attributed to Ru^0–CO.[24,25] A significant decrease in band intensity was observed for all spent catalysts compared to fresh Ru/

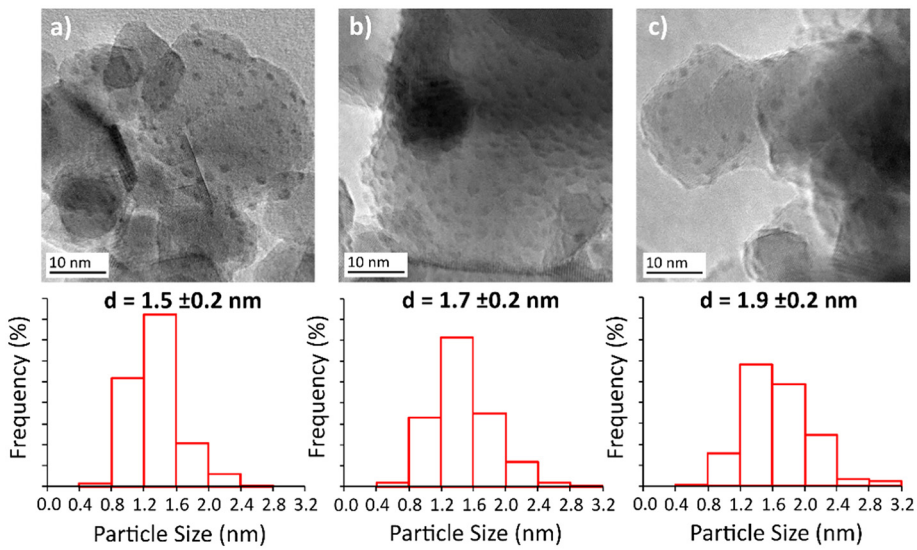

Fig. 3 TEM images and the corresponding histograms of the Ru nanoparticle size distribution with the mean particle size for (a) the fresh Ru/TiO_2 catalyst, and for the spent catalysts used in (b) dioxane and (c) water.

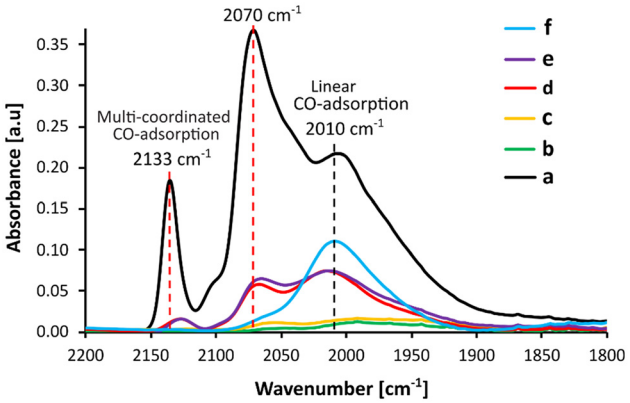

Fig. 4 CO-adsorbed FTIR spectra of (a) the fresh Ru/TiO_2 catalyst, and of the spent catalysts used in (b) pure dioxane, (c) 10% water, (d) 50% water, (e) 90% water, and (f) pure water.

TiO_2, indicating that the Ru sites became less accessible after the reaction, possibly due to surface coverage by carbonaceous residues.[25] This observation aligns well with the FTIR spectra of the spent catalysts collected after reaction in pure dioxane and pure water (Fig. S3), which show a broad band in the 3700–3000 cm^{-1} region, characteristic of –OH stretching, and bands in the of 3000–2780 cm^{-1} range typically corresponding to C–H vibrations, demonstrating the presence of organic species on the catalyst surface. In the CO-adsorbed spectra of the catalysts after reaction in pure dioxane and in dioxane with low water content (10% H_2O), CO bands were almost completely suppressed compared to the fresh catalyst, suggesting extensive coverage of Ru sites by strongly adsorbed substrate, reaction products, or solvent. Indeed, dioxane itself can adsorb on the catalyst surface, further contributing to site blockage and reduced CO accessibility.[26] In contrast, catalysts after reaction in higher water content solvents (50% and 90% H_2O) retained the bands associated with both multi-coordinated and linear CO adsorption, indicating that water plays a critical role in preserving Ru surface availability. For the catalyst spent in pure water, an intense band corresponding to linear CO adsorption was observed, while the bands associated with multi-coordinated CO adsorption on oxidized Ru disappeared. This spectral change indicates that water contributes to preserving the availability of surface Ru sites and promotes a higher proportion of metallic Ru. Similar trends were observed for the four-times-cycled Ru/TiO_2 catalysts after extended cycling in pure water and pure dioxane (Fig. S2).

XPS studies were also carried out on both fresh and spent samples to further probe the surface composition of the Ru/TiO_2 catalysts (Fig. S4). In the fresh catalyst, the Ru 3d primary region spectra confirmed the presence of both Ru^0 and Ru^{4+} species, in agreement with previous studies on various supports.[27–30] Two Ru 3d5/2–Ru 3d3/2 orbital doublet contributions were observed at 280.2 eV and 281.9 eV with a 4.1 eV spin orbit splitting, in addition to the contributions from adventious carbon at higher binding energy (Fig. S4B). We assume that the presence of Ru^{4+} species resulted from natural surface oxidation, as metallic Ru undergoes oxidation very easily upon air exposure. The catalyst exhibited a high Ru/Ti surface atomic ratio of 0.027, consistent with the small, well-dispersed and uniform Ru nanoparticles observed by TEM. Additionally, the Cl 2p XPS spectra (Fig. S4D) revealed the presence of residual chlorine species on the surface of the fresh catalyst, consistent with the observations of Mazzieri *et al.* who reported Ru oxychloride species on the support surface when $RuCl_3$ was used as the precursor for catalyst preparation.[31] After the catalytic test, a pronounced attenuation of the Ru signal was observed in the spent catalysts recovered from water and from dioxane, accompanied by a strong increase in the multi-component C 1s orbital envelope. However, within the accuracy of the measurement, only a negligible decrease in the Ru/Ti surface atomic ratio was observed, down to 0.026 and 0.024 for the catalysts tested in water and in dioxane, respectively, as a concomitant decrease in the Ti 2p signal was observed (Fig. S4C). This behavior likely reflects a non-selective deposition of carbonaceous species during the reaction, affecting both the Ru sites and the TiO_2 support. In addition, no residual surface chlorine was detected, at the sensitivity limit of the technique, indicating a significant release of chlorine species during the reaction. Since Ru leaching during the reaction was negligible (Table S3) and TEM showed only a slight increase in particle size, the drastic reduction of the Ru signal is therefore attributed to extensive carbon deposition on the catalyst surface, consistent with the ToF-SIMS results.

The presence of carbon deposits on the catalyst surface, as well as their influence on the availability of Ru sites, was confirmed by ToF-SIMS analysis. Fig. 5 shows the normalized intensities of selected ions from the surfaces of the fresh and spent Ru/TiO_2 catalysts. The relative intensity of C^+ ions was very low for the fresh catalyst, whereas catalysts spent in pure dioxane and 10% water exhibited the highest relative intensity of C^+ ions among all samples, suggesting substantial accumulation of carbonaceous species over the catalyst surface.

The corresponding C/Ru ratios were also the highest, confirming that Ru sites were extensively masked by carbon residues, in good agreement with the CO-FTIR results. A similar trend was observed for the C/TiO ratio (Fig. S5a), indicating that carbon deposits formed not only on Ru sites but also broadly across the TiO_2 support. When the water content in the reaction medium increased, both the C^+ ion intensity and the C/Ru ratio decreased by at least a factor of two, demonstrating that water mitigates the accumulation of carbon residues and hence helps in preserving the accessibility to Ru sites, consistent with the CO-FTIR findings. Furthermore, chlorine species originating from precursor residues were detected on the surface of the catalysts. The chlorine signal was most pronounced for the fresh sample, decreased for the sample used in dioxane, and was the lowest for the catalysts tested in solvent mixtures containing at least 50% of water (Fig. S5b). This discrepancy with the XPS results likely arises from the much smaller analysis depth in ToF-SIMS compared to that of XPS, as also reported by Ivanez *et al.* for Ru/TiO_2 systems.[28]

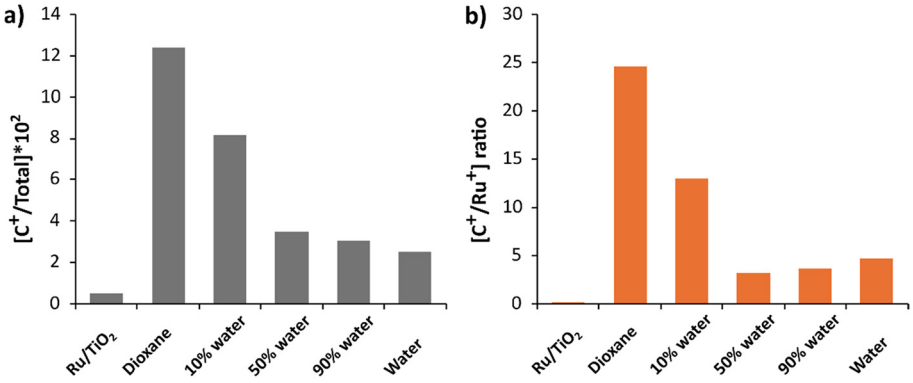

Fig. 5 Normalized intensities of selected ions obtained from ToF-SIMS spectra of the Ru/TiO_2 catalysts spent in different reaction media, (a) C^+ and (b) C^+/Ru^+.

The reducibility of the fresh and spent catalysts was investigated using TPR (Fig. 6). In the case of the fresh Ru/TiO_2 catalyst, the reduction peak at a temperature of 147 °C is characteristic of the reduction of Ru^{3+} and Ru^{2+} species to metallic Ru.[32,33] For all the spent catalysts, a decrease in the reduction temperature was systematically observed compared to the fresh sample (147 °C), with the effect becoming more pronounced as the water content increased, down to 120 °C for the catalyst used in pure dioxane and to 90 °C for those tested in solvent mixtures containing more than 50% water. These changes directly correlate with the amount of residual chlorine detected on the catalyst surface (ToF-SIMS, XPS). Chlorine is known to strongly stabilize ruthenium in its oxidized state, thereby hindering its reduction.[34] Moreover, by influencing the metal–support interaction, chlorine can further slow down the reduction process, which could explain the higher reduction temperature observed for the fresh sample and the lower one after reaction in the presence of water.[34] However, we cannot rule out that the slightly larger Ru particle size observed in the spent catalysts may also result to more weakly interacting Ru species, which would consequently be more easily reducible than those in the fresh catalyst.

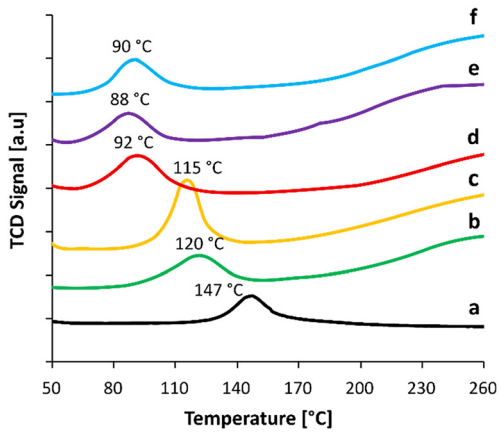

Fig. 6 TPR profiles of (a) the fresh Ru/TiO_2 catalyst, and of the spent Ru/TiO_2 catalyst used in (b) pure dioxane, (c) 10% water, (d) 50% water, (e) 90% water, and (f) pure water.

3.3 Investigating the reaction mechanism

To gain molecular-level insights into the reaction mechanism and the role of water in the production of HHD and 1,2,5-HT, the reaction profiles were evaluated using periodic DFT calculations and a Ru(0001) surface as a model of the main surface sites of the Ru/TiO_2 catalyst. Since the branching point is located after the production of BHMF, our mechanistic analysis was focused downstream this intermediate. Three main reaction pathways were identified (Scheme 1):

Path 1: ring-opening to generate various compounds such as HHD, 1,2,5-HT, *etc*.

Path 2: ring hydrogenation to produce BHMTHF.

Path 3: carbon hydroxyl (C–OH) bond cleavage to form 5-MFA and further downstream compounds like dimethylfuran (DMF).

Since the formation of 5-MFA and DMF requires harsher reaction conditions, as confirmed by the absence of C–OH bond cleavage downstream products and the excellent carbon balance, the contribution of **Path 3** is considered negligible under our reaction conditions, and hence this pathway was not further investigated. According to our experimental findings, **Path 2** (formation of BHMTHF) is preferred when using dioxane as a solvent, while **Path 1** (ring-opening route, formation of HHD) is favored in aqueous conditions. In this work, we focus on the detailed mechanism of **Path 1** to elucidate why it is preferred in water.

During the hydrogenolysis of BHMF to HHD and 1,2,5-HT, not only the ring is opened, but also the oxygens are shuffled along the carbon skeleton. In HHD, the oxygen atoms are located at the 1st, 2nd, and 5th positions of the molecule, while opening the ring of BHMF yields intermediates with oxygen atoms at the 1st, 2nd, and 6th positions. Since our experimental results show no evidence for the formation of linear C_6 derivatives with the 1/2/6 substitution pattern, the necessary OH shuffling likely happens at the catalyst surface rather than in the bulk solution. Besides, this surface process is clearly facilitated by the pres-

ence of water that is known to be activated by Ru, yielding surface hydroxyl OH and H (OH* and H*) with an exergonic reaction energy of 0.6 eV.[17,35–37] These considerations indicate that the oxygen atom at the 5th position in HHD likely originates from an external source, namely the water solvent. In short, three main processes occur in **Path 1**: (i) the opening of the furan ring; (ii) the addition of OH*, forming a new C–O bond; (iii) the cleavage of one of the terminal C–O bonds. Since C–O scission products such as 5-MFA or DMF were not observed, we discarded the possibility of starting with the latter process. Two possibilities remain: (i) starting with the furan ring-opening or (ii) starting with the addition of OH*.

First, we explored the route starting with the addition of OH* and H* onto the double bond in the furan ring of BHMF. We identified two possible regio-isomers, **Int-A** and **Int-B**, depending on which carbon is added OH* and H*. In both cases, the reaction is strongly endergonic (>1.5 eV, see Fig. S6), preventing it from being a feasible route.

Then, we explored the route starting with the ring-opening of BHMF, yielding **Int-C**. This is favoured by an exothermic reaction energy (DG = −0.40 eV) and a low activation energy barrier of 0.54 eV. This is consistent with the findings of Gilkey *et al.*, who reported that dimethyl furan, having a similar ring structure, also favours an open-ring conformation on the Ru surface.[38] We evaluated the influence of the inclusion of the solvent as a continuum model on that step (see Table S5) and found that is was very limited (variation of less than 0.03 eV on the activation barrier). This shows that a continuum is not key to rationalizing solvent effect for this kind of reaction, in agreement with previous findings.[39] Including direct participation of water is necessary. This is done here by considering the possible dissociation of water that generates OH* and H*, and the subsequent reactions that involve OH* as a reactant. Then, to shuffle the positions of the OH groups, a C–OH bond needs to be formed, prior or after a C–OH bond scission, as illustrated in Scheme 2. The corresponding reaction profiles are shown in Fig. 7, with the intermediates and transition state structures shown in Fig. S7 and Fig. 8, respectively. Forming the C–OH first yields **Int-D**, while the C–OH cleavage generates **Int-E** (its regioisomer, where the other OH terminal is cleaved, was found to be less stable by 0.21 eV). Then, the two paths converge to **Int-F-a/Int-F-b**, where the OH are positioned on the 1st, 2nd, and 5th positions of the molecule, as in the intermediate product HHD. **Int-F-b** is clearly easier to reach than **Int-F-a** (0.93 *vs.* 1.60 eV activation energy) from **Int-D** and can also be obtained from **Int-E**. Then, this enol can easily tautomerize to its keto form **Int-G** to finally be hydrogenated into **HHD** and then 1,2,5-HT.

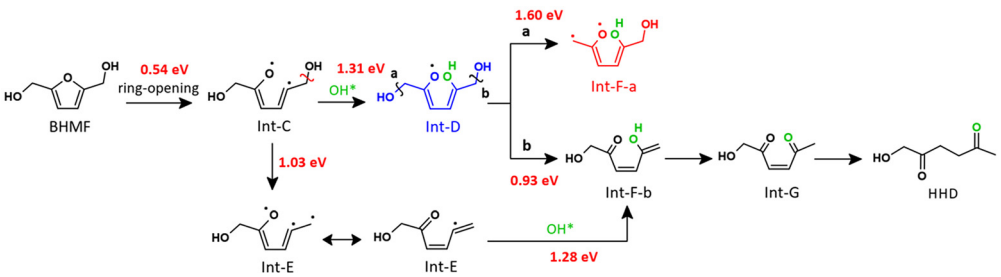

Scheme 2 Reaction mechanism of HHD formation from BHMF, starting with the ring-opening of BHMF (Path 1).

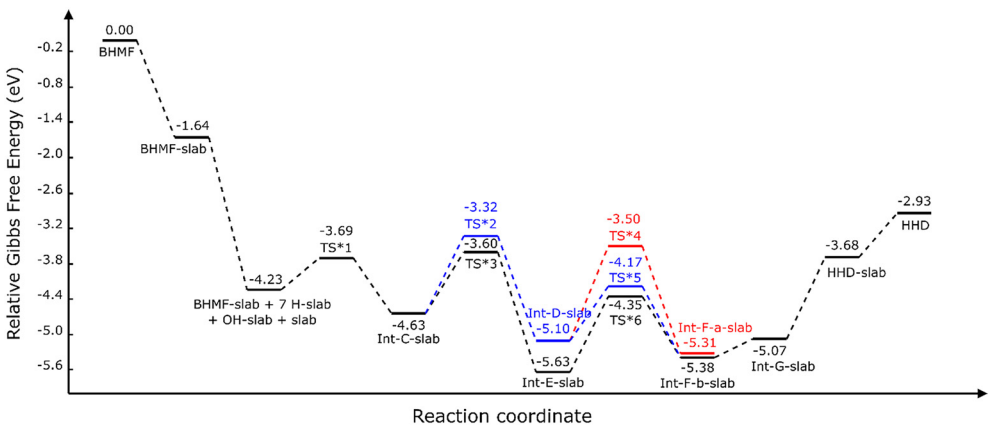

Fig. 7 Gibbs energy pathway (T = 120 °C, in eV) of Path 1, corresponding to the conversion of BHMF into HHD on Ru(0001) in the presence of H_2 and water. A dissociative adsorption of H_2 and H_2O is assumed on the Ru(0001) slabs. The reference state corresponds to 1 BHMF, 1 H_2O, and 3 H_2 molecules and 10 Ru(0001) slabs.

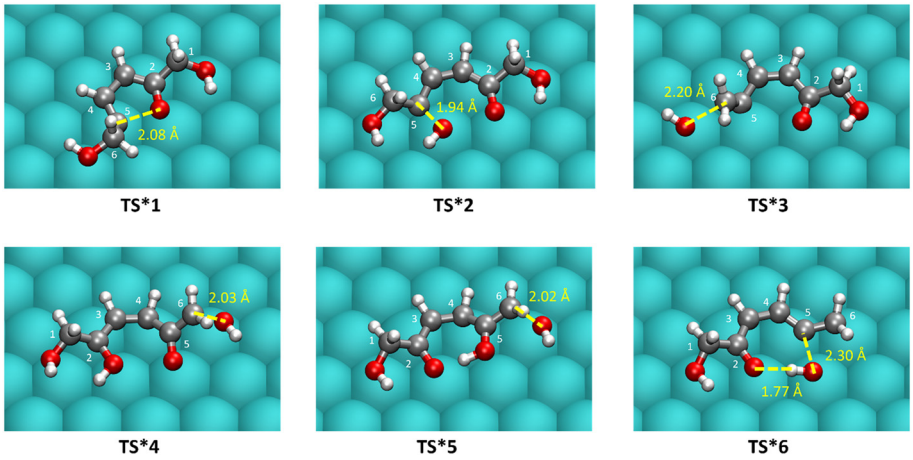

Fig. 8 Top view of the optimized structures of **TS*1** to **TS*6**. The C···OH distance is provided in Å. Other key distances are provided in Tables S6 and S7. Ru in cyan blue, C in grey, O in red, and H in white. The surface and organic part are shown using a van der Waals and ball-and-stick representation, respectively.

The two ways to shift the terminal OH from the 6th to the 5th position are in competition, and there is no clear dominant path. In both ways, the C_5–OH bond formation is the limiting step. Making this bond in **Int-C** is an exergonic process (DG = −0.43 eV). However, this process is associated with a significant activation barrier of 1.31 eV that may be related to the changes in the Ru/C_5 interactions in **TS*2**: the C_5 atom needs to shift from a bridge position in **Int-C**, in strong interaction with the ruthenium surface (C_5–Ru = 2.07 Å, 2.16 Å), to an almost top position in **Int-D**, with a weaker interaction (C_5–Ru = 2.29 Å, 2.81 Å). A similar situation is found when making the C_5–OH bond in **Int-E**. In this intermediate, the C_5 carbon is also in strong interaction with the ruthenium surface, adsorbed in a hollow-like site with Ru–C_5 = 2.06 Å; 2.28 Å; 2.43 Å. It needs to shift to a top position in **TS*6** (Ru–C_5 = 1.96 Å) to reach **Int-F-b**, where it interacts weakly with 3 Ru surface atoms (Ru–C_5 = 2.45 Å; 2.73 Å; 2.82 Å). Despite a stabilizing H-bond (OH···O = 1.77 Å), reaching **TS*6** requires to overcome a barrier of 1.28 eV. Since in both ways the C-OH bond formation is the limiting step and features a barrier above 1.2 eV (**TS*2**, **TS*6**), the corresponding rate is directly influenced by the concentration of OH*: the higher the surface concentration of OH*, the higher the rates to form a C–OH bond. While this concentration is negligible in pure dioxane, it is expected to increase with the increase in water content, thanks to the easy water dissociation on Ru.[17,35–37] This is why the production of HHD is facilitated in water compared with dioxane.

During the catalytic tests, we observed that the initial conversion of HMF to HHD occurs rapidly, reaching complete HMF conversion and about 90% HHD yield within 140 min. In contrast, the subsequent hydrogenation of HHD to 1,2,5-HT proceeds much more slowly. GC-MS analysis of the reaction mixture during this stage revealed the presence of intermediate compounds, indicating that the reaction pathways are more complex than straightforward hydrogenation. To better understand the origin and nature of these intermediates, we turned to DFT calculations. The computations suggest that hydrogenation of HHD can proceed *via* two possible intermediates: **Int-H**, formed by reduction at the 5th position, and **Int-I**, resulting from hydrogenation at the 2nd position to give a 1,2-diol. Among these, the pathway *via* **Int-I** is energetically more favorable by 0.17 eV (Fig. S8). Importantly, once **Int-I** forms, it can undergo a pinacol–pinacolone rearrangement under the acidic reaction conditions to generate a rearranged carbonyl intermediate (**Int-J**), which may subsequently react to form acetal-type compounds, as illustrated in Scheme 3. These computational insights provide a coherent explanation for the complex mixture observed experimentally and rationalize the slower conversion of HHD to 1,2,5-HT.

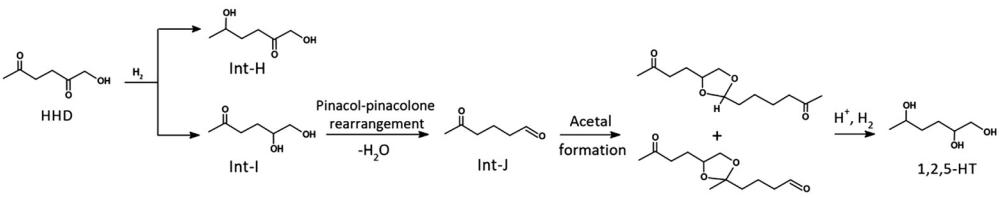

Scheme 3 Possible reaction intermediates, namely the diol 5,6-dihydroxyhexan-2-one (**Int-I**) and the carbonyl compound 5-oxohexanal (**Int-J**), as well as acetal intermediates involved in the conversion of HHD to 1,2,5-HT.

The importance of **Int-J** is strongly supported by GC-MS data, which shows a compound with a molecular weight of 114, which corresponds to **Int-J** ($C_6H_{10}O_2$). Its fragmentation spectrum shows a prominent peak at *m*/*z* 43, characteristic of the CH_3CO^+ ion, confirming the presence of a carbonyl-containing intermediate (Fig. S9a).[40] In addition, a higher molecular weight species at *m*/*z* 228 was observed, attributed to an acetal derivative formed from **Int-J**. The mass spectrum of this species also shows a strong base peak at *m*/*z* 43, confirming that it is derived from the **Int-J** intermediate, and features a fragment at *m*/*z* 198 resulting from the loss of a formaldehyde group (Fig. S9b). Other detected fragments at *m*/*z* 55 and 85 are attributed to chain or ring cleavages adjacent to carbonyl or ether groups, while fragments at *m*/*z* 96 and 98 likely arise from carbonyl or hydroxyl-containing fragments.[41] Thus, the MS signals align well with the proposed reaction intermediates, demonstrating that the acetals can break down further under hydrogenation conditions to form 1,2,5-HT as the final hydrogenated product.

4. Discussion

4.1 Role of water

Our experimental data show that careful tuning of the water-dioxane solvent ratio can direct the reaction towards either selective ring hydrogenation or ring-opening products. In both solvents, BHMF is a key intermediate. In pure dioxane, we obtained BHMTHF, which results from the selective hydrogenation of the furan ring of BHMF. By contrast, the presence of water shifts the reaction toward ring-opening products such as HHD and 1,2,5-HT. A gradual increase in water content progressively decreases the yield of ring-hydrogenated products and facilitates the synthesis of ring-opening products, as illustrated in Fig. 9.

The detailed mechanism was studied using DFT computations to further understand the experimentally observed solvent-dependent product distributions. The conversion of the BHMF intermediate to ring-opening products (HHD and 1,2,5-HT) proceeds mainly through a water-assisted rearrangement of the OH groups from a 1,2,6 substitution pattern in the ring-opening intermediate **Int-C** to the 1,2,5 pattern in HHD and 1,2,5-HT. This OH shift from the C_6 to the C_5 position requires breaking and making C–OH bonds. The formation of the C_5–OH bond is the limiting step (activation energy above 1.2 eV through **TS*2** or **TS*6**), and the corresponding rate is very sensitive to the availability of surface hydroxyl species (OH*). Since water can easily dissociate into OH* and H* at the Ru/water interface, the surface concentration of OH* increases with an increasing water content. Hence, the formation of HHD is selectively enhanced in aqueous media. This active participation of water in the furan ring-opening is strongly supported by the work of Ramos *et al.*, who demonstrated that the water molecules participate in the BHMF ring-opening to yield HHD *via* a hydration-dehydration step using isotopic labelling experiments with D_2O as solvent.[42] Similarly, in the investigation of the conversion of furfural to 1,2-pentanediol using Pt-based catalysts, Ma *et al.* found that water significantly enhanced selectivity toward 1,2-pentanediol compared to reactions conducted in purely organic solvents like methanol or THF, where the process primarily yielded the partially hydrogenated compound that is furfural alcohol. By combining DFT calculations with isotope tracing ($H_2{}^{18}O$) experiments, they showed that water molecules adsorb adjacent to the ring-opening intermediates on the Pt(111) surface, with the oxygen from water directly incorporating into the 1,2-pentanediol product.[43] This highlights the active chemical participation of water in the reaction pathway.

Our mechanism is in qualitative agreement with the mechanistic study by Zhu *et al.*, on the conversion of HMF to HHD using a Pd–Au/TiO_2 catalyst. Their investigations demonstrated that the reaction likewise proceeds *via* hydrolytic ring-opening of the furan ring in BHMF, generating a key keto intermediate equivalent in structure and function to our **Int-G**. To probe this pathway further, they used a model compound, 4-(5-methyl-2-furyl)-3-butene-2-one (MFBTO), to mimic the proposed ring-opened intermediate, since the actual intermediate was too reactive to isolate. They found that the hydrogenation rate of MFBTO was approximately ten times higher than that of HMF, which explains why the open-chain keto intermediate could not be directly detected in their reaction mixture; rather, the further hydrogenated product (HHD) was obtained.[12] These findings are fully consistent with our results, reinforcing the formation of **Int-G** in the water-assisted ring-opening pathway for HHD synthesis.

The presence of carbonaceous residues on the spent catalyst surface was directly demonstrated using ToF-SIMS and indirectly using CO-adsorbed infrared spectroscopy and XPS analysis. Fig. 10(a) shows a clear correlation between the amount of carbon species accumulated on the spent Ru/TiO_2 catalysts and the percentage of dioxane in the reaction media, with the highest C^+ ion intensity observed for the pure dioxane case. This trend is consistent with the influence of the water content on the accessibility of metallic Ru sites in the spent

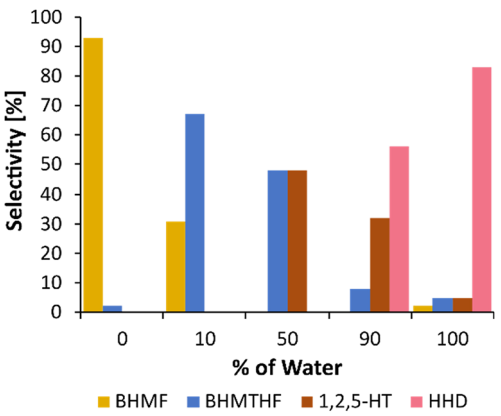

Fig. 9 Influence of water on the selectivity in HMF hydrodeoxygenation over Ru/TiO_2 after 150 min at 120 °C under 70 bar H_2.

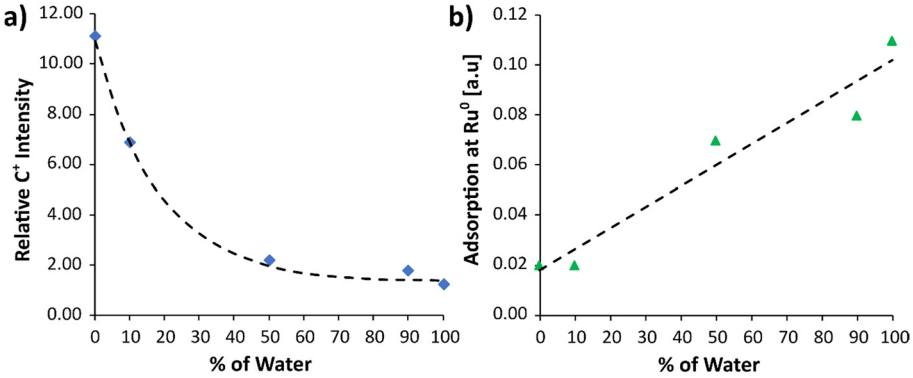

Fig. 10 Influence of water on (a) the relative intensity of carbon residues determined by ToF-SIMS and (b) the intensity of CO-adsorption on metallic Ru sites at wavenumber 2010 cm^{-1} for the spent Ru/TiO_2 catalysts. The dotted lines serve as an eye-guiding aid to visualize the trends.

Ru/TiO_2 catalyst, as evidenced by CO adsorption bands in the infrared spectroscopy shown in Fig. 10(b) and XPS spectra. The catalyst used in pure dioxane and in a 10% water mixture exhibited the lowest availability of metallic Ru sites for CO-adsorption, while higher water contents preserved Ru site accessibility, as indicated by stronger CO adsorption intensities. The substantial carbon accumulation observed in the absence of water is most likely due to the strong adsorption of reaction intermediates such as BHMF, but also **Int-C** or **Int-E**, which cannot be further converted into **HHD** when the surface concentration in OH* is low (see the DFT results in Scheme 2 and Fig. 7). In addition, the solvent (dioxane) itself may also interact with and partially block Ru sites.[26]

4.2 Role of dioxane

It is worth noting that in pure dioxane the reaction affords 100% BHMTHF, and no HHD is detected, whereas in pure water the opposite trend is observed. However, an intermediate 1 : 1 water–dioxane mixture lowers the selectivity toward HHD and increases the formation of 1,2,5-HT compared to pure water or 90% water. This indicates a faster hydrogenation rate in the mixed solvent system and highlights the importance of H_2 solubility in determining product distribution.[44,45]

To verify the role of H_2 in different solvents, experiments at different stirring rates ranging from 350 to 1000 rpm effectively demonstrated that H_2 mass transfer limits the reaction under aqueous conditions (Tables S8 and S9).[46] In dioxane, the reaction rate remained essentially unaffected by stirring speed, while in water it was markedly lower at low stirring rates and increased with higher agitation. This behavior is consistent with literature reports.[47,48]

Further confirmation was obtained from experiments using HHD as the substrate (Table S10). The formation of 1,2,5-HT proceeded more rapidly in pure dioxane and in the dioxane–water mixture than in pure water. This indicates that the higher yields of fully hydrogenated products in the mixed solvent system most likely arise from enhanced H_2 availability compared with water alone.

Although dioxane is not as influential as water in determining overall selectivity direction from HMF, it provides a beneficial increase in H_2 solubility that facilitates further hydrogenation to 1,2,5-HT.

5. Conclusions

In this work, we demonstrate that the overall product distribution in HMF hydrodeoxygenation using Ru/TiO_2 catalyst can be effectively controlled by tuning the solvent, which modulates the relative rates of hydrogenation and C–OH bond formation. BHMTHF is favored by a fast hydrogenation rate, which can be obtained using dioxane. HHD is preferentially formed in pure water, where the hydrogenation steps are slow, and the OH bond-breaking/bond formation steps are promoted by a high concentration of surface OH*. Finally, 1,2,5-HT is favored when both processes are competitive, requiring a sufficient concentration of H_2 in the solvent and a high enough surface concentration in OH*, namely in our case when using a 1 : 1 mixture of dioxane and water. Moreover, we show for the first time that a high yield of 1,2,5-HT (75%) can be obtained using Ru/TiO_2 in a one-pot reaction conducted in a pure aqueous system. The catalyst also exhibits good recyclability over multiple cycles, maintaining high activity and selectivity in both solvents.

Author contributions

Preeti Kashyap: writing – original draft, visualization, investigation, formal analysis; Marcin Jędrzejczyk: investigation; Mingjun Gu: investigation, visualization; Stephan N. Steinmann: writing – review & editing; David Kubička: writing – review & editing; Nicolas Keller: investigation, writing – original draft, visualization; Carine Michel: methodology, software, writing – original draft, writing – review & editing, supervision, resources, data curation; Agnieszka M. Ruppert: methodology, writing – original draft, writing – review & editing, visualization, supervision, resources, project administration, investigation, funding acquisition, conceptualization.

Conflicts of interest

There are no conflicts to declare.

Data availability

Supplementary information (SI) contains additionnal catalytic tests, CO-adsorbed FTIR spectra, XRD, XPS, ToF-SIMS, further experimental details, and theoretical investigations. The optimized geometries from DFT calculations are available through the online database at https://doi.org/10.17172/NOMAD/2026.01.10-1. The metadata for the experimental part are available through the online database at https://doi.org/10.34658/RDB.GGLYR5. See DOI: https://doi.org/10.1039/d5gc06439b

Acknowledgements

The National Center of Science (NCN), Krakow, Poland, is gratefully acknowledged for financially supporting work through an OPUS-LAP grant (2020/39/I/ST4/02039). David Kubička acknowledges the funding from the Czech Science Foundation (Project No. GF21-45648 L). M. Gu, S. N. Steinman, and C. Michel acknowledge financial support from the ANR (TERS_NORMAL ANR-22-CE29-0027) and support from the CBPsmn (PSMN, Pôle Scientifique de Modélisation Numérique) of the ENS de Lyon for the computing resources. The authors thank F. Filippi for insightful discussion on H_2 solubility in mixture of solvents. P. Kashyap was the Doctoral Candidate in the Interdisciplinary Doctoral School at the Lodz University of Technology, Poland.

References

1 P. Mäki-Arvela, D. Ruiz and D. Y. Murzin, *ChemSusChem*, 2021, **14**, 150–168.
2 M. Przydacz, P. Kashyap, N. Tanchoux, D. Ihiawakrim, D. Kubička, N. Keller and A. M. Ruppert, *ChemCatChem*, 2025, **17**, e202401818.
3 P. Kashyap, M. Jędrzejczyk, M. Akhgar, J. Aubrecht, D. Kubička, N. Keller and A. Ruppert, *ChemCatChem*, 2025, **17**, e202401433.
4 Z. Huang, J. Wang, J. Lei, W. Zhao, H. Chen, Y. Yang, Q. Xu and X. Liu, *Front. Chem.*, 2022, **10**, 1–8.
5 X. Tang, J. Wei, N. Ding, Y. Sun, X. Zeng, L. Hu, S. Liu, T. Lei and L. Lin, *Renewable Sustainable Energy Rev.*, 2017, **77**, 287–296.
6 S. Nishimura, S. Ohmatsu and K. Ebitani, *Fuel Process. Technol.*, 2019, **196**, 106185.
7 B. Wozniak, S. Tin and J. G. De Vries, *Chem. Sci.*, 2019, **10**, 6024–6034.
8 C. Zhang, Y. Li, X. Lv, X. Gao, Y. Duan, D. Sui and Y. Yang, *ChemistrySelect*, 2022, **7**, e202103797.
9 G. C. A. Luijk, N. P. M. Huck, F. van Rantwijk, L. Maat and H. van Bekkum, *Heterocycles*, 2009, **77**, 1037–1044.
10 Y. Yang, D. Yang, C. Zhang, M. Zheng and Y. Duan, *Molecules*, 2020, **25**, 2475.
11 F. Liu, M. Audemar, K. De Oliveira Vigier, J. M. Clacens, F. De Campo and F. Jérôme, *ChemSusChem*, 2014, **7**, 2089–2093.
12 M. M. Zhu, X. L. Du, Y. Zhao, B. B. Mei, Q. Zhang, F. F. Sun, Z. Jiang, Y. M. Liu, H. Y. He and Y. Cao, *ACS Catal.*, 2019, **9**, 6212–6222.
13 Y. Duan, M. Zheng, D. Li, D. Deng, L. F. Ma and Y. Yang, *Green Chem.*, 2017, **19**, 5103–5113.
14 L. Longo, S. Taghavi, E. Ghedini, F. Menegazzo, A. Di Michele, G. Cruciani and M. Signoretto, *ChemSusChem*, 2022, **15**, e202200437.
15 D. Polidoro, I. E. Mihai, A. Perosa and M. Selva, *ACS Sustainable Chem. Eng.*, 2023, **11**, 2520–2530.
16 C. Michel, J. Zaffran, A. M. Ruppert, J. Matras-Michalska, M. Jędrzejczyk, J. Grams and P. Sautet, *Chem. Commun.*, 2014, **50**, 12450–12453.
17 C. Michel and P. Gallezot, *ACS Catal.*, 2015, **5**, 4130–4132.
18 J. Sebastian, C. Mebrahtu, F. Zeng and R. Palkovits, *Angew. Chem., Int. Ed.*, 2026, **65**, e02611.
19 S. Doniach and M. Sunjic, *J. Phys. C:Solid State Phys.*, 1970, **3**, 285.
20 D. A. Shirley, *Phys. Rev. B*, 1972, **5**, 4709–4714.
21 J. H. Scofield, *J. Electron Spectrosc. Relat. Phenom.*, 1976, **8**, 129–137.
22 H. Wang, Z. Gao, B. Sun, S. Mu, F. Dang, X. Guo, D. Ma and C. Shi, *Chem. Catal.*, 2023, **3**, 100768.
23 S. J. Turner, N. L. Visser, R. Dalebout, D. F. L. Wezendonk, P. E. de Jongh and K. P. de Jong, *Small*, 2024, **20**, 1–10.
24 K. Hadjiivanov, J. C. Lavalley, J. Lamotte, F. Maugé, J. Saint-Just and M. Che, *J. Catal.*, 1998, **176**, 415–425.
25 N. M. Gupta, V. P. Londhe and V. S. Kamble, *J. Catal.*, 1997, **169**, 423–437.
26 F. Héroguel, X. T. Nguyen and J. S. Luterbacher, *ACS Sustainable Chem. Eng.*, 2019, **7**, 16952–16958.
27 A. M. Ruppert, M. Jędrzejczyk, O. Sneka-Płatek, N. Keller, A. S. Dumon, C. Michel, P. Sautet and J. Grams, *Green Chem.*, 2016, **18**, 2014–2028.
28 J. Ivanez, P. Garcia-Munoz, A. M. Ruppert and N. Keller, *Catal. Today*, 2021, **380**, 138–146.
29 A. Kim, C. Sanchez, G. Patriarche, O. Ersen, S. Moldovan, A. Wisnet, C. Sassoye and D. P. Debecker, *Catal. Sci. Technol.*, 2016, **6**, 8117–8128.
30 M. Chen, Y. Huang, H. Pang, X. Liu and Y. Fu, *Green Chem.*, 2015, **17**, 1710–1717.
31 V. Mazzieri, F. Coloma-Pascual, A. Arcoya, P. C. L'Argentière and N. S. Fígoli, *Appl. Surf. Sci.*, 2003, **210**, 222–230.
32 S. Masuda, K. Mori, T. Sano, K. Miyawaki, W. H. Chiang and H. Yamashita, *ChemCatChem*, 2018, **10**, 3526–3531.
33 W. Tolek, N. Nanthasanti, B. Pongthawornsakun, P. Praserthdam and J. Panpranot, *Sci. Rep.*, 2021, **11**, 9786.
34 J. M. Crawford, B. E. Petel, M. J. Rasmussen, T. Ludwig, E. M. Miller, S. Halingstad, S. A. Akhade, S. H. Pang and M. M. Yung, *Appl. Catal., A*, 2023, **663**, 119292.

35 P. J. Feibelman, *Science*, 2002, **295**, 99–102.
36 C. Michel, F. Göltl and P. Sautet, *Phys. Chem. Chem. Phys.*, 2012, **14**, 15286–15290.
37 H. Li, Z. W. Wang, S. Zhang, G. L. Li, W. Ju, T. Li and L. Li, *Phys. E*, 2021, **131**, 114730.
38 M. J. Gilkey, A. V. Mironenko, L. Yang, D. G. Vlachos and B. Xu, *ChemSusChem*, 2016, **9**, 3113–3121.
39 B. Schweitzer, S. N. Steinmann and C. Michel, *Phys. Chem. Chem. Phys.*, 2019, **21**, 5368–5377.
40 R. A. Friedel and A. G. Sharkey, *Anal. Chem.*, 1956, **28**, 940–944.
41 K. Woelfel and T. G. Hartman, *ACS Symp. Ser.*, 1998, **705**, 193–210.
42 R. Ramos, A. Grigoropoulos, B. L. Griffiths, A. P. Katsoulidis, M. Zanella, T. D. Manning, F. Blanc, J. B. Claridge and M. J. Rosseinsky, *J. Catal.*, 2019, **375**, 224–233.
43 R. Ma, X. P. Wu, T. Tong, Z. J. Shao, Y. Wang, X. Liu, Q. Xia and X. Q. Gong, *ACS Catal.*, 2017, **7**, 333–337.
44 S. Fulignati, C. Antonetti, D. Licursi, M. Pieraccioni, E. Wilbers, H. J. Heeres and A. M. Raspolli Galletti, *Appl. Catal., A*, 2019, **578**, 122–133.
45 S. Lima, D. Chadwick and K. Hellgardt, *RSC Adv.*, 2017, **7**, 31404–31407.
46 H. Hu, A. Ramzan, R. Wischert, F. Jerôme, C. Michel, K. de Olivera Vigier and M. Pera-Titus, *Catal. Sci. Technol.*, 2021, **11**, 7973–7981.
47 D. W. Flaherty, *ACS Catal.*, 2018, **8**, 1520–1527.
48 Z. Zhu, Y. Cao, Z. Zheng and D. Chen, *Energies*, 2022, **15**, 5021.